A new method for obtaining transparent electrodes

Malureanu, Radu; Zalkovskij, Maksim; Song, Zhengyong; Gritti, Claudia; Andryieuski, Andrei; He, Qiong; Zhou, Lei; Jepsen, Peter Uhd; Lavrinenko, Andrei

Published in:
Optics Express

Link to article, DOI:
10.1364/OE.20.022770

Publication date:
2012

Document Version
Publisher's PDF, also known as Version of record

A new method for obtaining transparent electrodes

Radu Malureanu,[1,3,*] **Maksim Zalkovskij,**[1,3] **Zhengyong Song,**[2,3] **Claudia Gritti,**[1] **Andrei Andryieuski,**[1] **Qiong He,**[2] **Lei Zhou,**[2] **Peter Uhd Jepsen,**[1] **and Andrei V. Lavrinenko**[1]

[1] *Department of Photonics Engineering, Technical University of Denmark, Kgs. Lyngby 2800, Denmark*

[2] *State Key Laboratory of Surface Physics, Key Laboratory of Micro and Nano Photonic Structures (Ministry of Education), Fudan University, Shanghai 200433, China*

[3] *These authors contributed equally to the work.*

**rmal@fotonik.dtu.dk*

Abstract: In this article, we propose a simple scheme to make a metallic film on a semi-infinite substrate optically transparent, thus obtaining a completely transparent electrode in a desired frequency range. By placing a composite layer consisting of dielectric and metallic stripes on top of the metallic one, we found that the back-scattering from the metallic film can be almost perfectly canceled by the composite layer under certain conditions, leading to transparency of the whole structure. We performed proof-of-concept experiments in the terahertz domain to verify our theoretical predictions, using carefully designed metamaterials to mimic plasmonic metals in optical regime. Experiments are in excellent agreement with full-wave simulations.

OCIS codes: (160.1245) Artificially engineered material; (160.3918) Metamaterials; (160.4760) Optical properties; (220.3740) Lithography; (220.4000) Microstructure fabrication; (230.4170) Multilayers; (240.3990) Micro-optical devices; (300.6495) Spectroscopy, terahertz; (310.4165) Multilayer design; (310.6188) Spectral properties; (310.6628) Subwavelength structures, nanostructures; (310.6805) Theory and design.

References and links

1. D. S. Hecht, L. Hu, and G. Irvin, "Emerging transparent electrodes based on thin films of carbon nanotubes, graphene, and metallic nanostructures," Adv. Mater. **23**, 1482–1513 (2011).
2. M. Vosgueritchian, D. J. Lipomi, and Z. Bao, "Highly conductive and transparent PEDOT:PSS films with a fluorosurfactant for stretchable and flexible transparent electrodes," Adv. Func. Mater. **22,** 421–428 (2012).
3. R. B. H. Tahar, T. Ban, Y. Ohya, and Y. Takahashi, "Tin doped indium oxide thin films: electrical properties," J. App. Phys. **83,** 2631–2645 (1998).
4. D. R. Cairns, R. P. Witte, D. K. Sparacin, S. M. Sachsman, D. C. Paine, G. P. Crawford, and R. R. Newton, "Strain-dependent electrical resistance of tin-doped indium oxide on polymer substrates," App. Phys. Lett. **76,** 1425–1427 (2000).
5. T. W. Ebbesen, H. J. Lezec, H. F. Ghaemi, T. Thio, and P. A. Wolff, "Extraordinary optical transmission through sub-wavelength hole arrays," Nature **391,** 667–669 (1998).
6. J. A. Porto, F. J. Garcia-Vidal, and J. B. Pendry, "Transmission resonances on metallic gratings with very narrow slits," Phys. Rev. Lett. **83**, 2845–2848 (1999).
7. H.-T. Chen, J. Zhou, J. F. OHara, F. Chen, A. K. Azad, and A. J. Taylor, "Antireflection coating using metamaterials and identification of its mechanism," Phys. Rev. Lett. **105,** 073901 (2010).
8. L. Zhou, W. Wen, C. T. Chan, and P. Sheng, "Electromagnetic-wave tunneling through negative-permittivity media with high magnetic fields," Phys. Rev. Lett. **94,** 243905 (2005).
9. Comsol Multiphysics by COMSOL ©, ver. 3.5, network license (2008).

#172483 - $15.00 USD Received 12 Jul 2012; revised 11 Sep 2012; accepted 12 Sep 2012; published 20 Sep 2012

10. D. Bergman, "The dielectric constant of a composite material - a problem in classical physics," Phys. Rep. **43**, 377–407 (1978).
11. K. Busch, C. T. Chan, and C. M. Soukoulis, in *Photonic Band Gap Materials* edited by C. M. Soukoulis (Kluwer, Dordrecht, 1996) **16**, 267–269 (1999).
12. J. B. Pendry, A. J. Holden, W. J. Stewart, and I. Youngs, "Extremely low frequency plasmons in metallic mesostructures," Phys. Rev. Lett. **76**, 4773–4776 (1996).
13. M. Naftaly, and R. E. Miles, "Terahertz time-domain spectroscopy of silicate glasses and the relationship to material properties," J. Appl. Phys. **102**, 043517 (2007).
14. CST ©Studio Suit, ver. 2011.
15. M. A. Ordal, L. L. Long, R. J. Bell, S. E. Bell, R. R. Bell, R. W. Alexander, Jr., and C. A. Ward, "Optical properties of the metals Al, Co, Cu, Au, Fe, Pb, Ni, Pd, Pt, Ag, Ti, and W in the infrared and far infrared," Appl. Opt., **22**,1099–1119 (1983).
16. N. J. Cronin, 'in *Microwave and Optical Waveguides* (Taylor & Francis, 1995).
17. C. A. Balanis, in *Advanced Electromagnetics Engineering* (Prentice Hall, 1989).
18. P. Yeh, in *Optical Waves in Layered Media* (Wiley Online library, 1988).

1. Introduction

For developing the new generation of electronic devices, varying from solar cells to electronic paper, touch screens, and displays, there is a clear need for transparent contact electrodes (TCEs) [1]. We define such contacts by their possibility of allowing a certain portion of the electromagnetic spectra of interest to pass through the contacts while, in the same time, maintaining the electrical connections intact. The research in this field is developed mainly towards transparent conductive oxides, conjugated polymers, colloidal semiconductors, and carbon allotropes in order to obtain low-cost and large-scale compatible electrodes [2]. Nowadays, the most promising material for TCEs is Indium-Tin-Oxide (ITO) [3]. Although it shows clear advantages with respect to its competitors, ITO comes with the inherent limitations. On one side, the scarcity and continuous increase in the price of indium, the main component of ITO is of great concern for an eventual implementation in the everyday devices. On the other, ITO is very brittle thus making devices like electronic paper or flexible screens difficult to achieve [4]. A different approach consists in using noble metals (such as Au, Ag etc.) to make TCEs. However, such materials are intrinsically opaque for light due to their high plasma frequency, and therefore, one has to structure these metals in various shapes to make them transparent within a certain frequency window [5, 6]. However, structuring may decrease the mechanical stability and electric conductivity of a metallic contact layer, what is undesired in practical applications. In addition, most previous efforts have been devoted to making free-standing TCEs, but in many real applications such as solar cells, the TCEs should function being deposited on a substrate, generally silicon (Si). In this case, the substrate itself having a high refractive index may induce substantial reflections, which should be avoided in applications. Therefore, it is highly desired to consider more realistic geometry when designing TCEs.

In [7], the authors suggest a new approach for fabricating anti-reflective coatings using Fabry-Perot resonances, where the cavity length is much smaller than the wavelength. Although our results in suppressing reflections are similar we are standing on other theoretical platform - scattering cancellation. The scattering cancellation method that we apply, can be, in principle, exploited to find the path to broadband functioning through the careful design of the top layer. We provide also an alternative route in designing of such structures based on the transmission line approach. It shows connection to both scattering cancellation and the Fabry-Perot models. Moreover, it allows to identify the most critical parameters influencing the bandwidth and the transparency window position.

In this work, we propose a simple scheme that can make a continuous and unstructured plasmonic metal film on top of a semi-infinite substrate, optically transparent in certain frequency windows. We first introduce the scheme and discuss the underlying physics in Sec. 2.

#172483 - $15.00 USD Received 12 Jul 2012; revised 11 Sep 2012; accepted 12 Sep 2012; published 20 Sep 2012

Specifically, as a proof of concept, we then choose the terahertz (THz) domain to verify our theoretical predictions (Section 3). An alternative transmission line model is introduced in Sec. 4. The model was validated in straight characterization. We describe the THz sample fabrication procedures in Sec. 5, and present our experimental results in Sec. 6, comparing them with the full wave simulation results. We conclude our paper in the last section.

2. Transparency by scattering cancellation - designing principle

Our scheme is inspired by early work [8] showing that an optically opaque layer (with a negative permittivity ε) can be perfectly transparent when sandwiched between two carefully designed metamaterial (MTM) layers. The physics behind obtaining the transparency is the cancellation of the scattering from the target opaque layer by carefully choosing the material and geometrical parameters of those two MTM layers. In the present problem, considering a continuous metal film C (with negative relative permittivity ε_C) on top of a semi-infinite substrate with relative permittivity ε_{sub}, our aim is to transmit in the most effective way electromagnetic (EM) waves through the C layer inwards the semi-infinite substrate. To achieve this goal we purposely placed a composite layer consisting of alternate A and B stripes (denoted as AB layer) on top of the C layer, as shown in Fig. 1(a). The width of the strips A and B are respectively denoted by w_A and w_B, and the periodicity of layer AB is $P = w_A + w_B$. Meanwhile, the thicknesses of layers AB and C are respectively d_{AB} and d_C.

To illustrate how the idea works, we performed full-wave numerical simulations based on the finite-element-method [9] to investigate the EM wave transmittance as functions of ε_B and P/λ. The results are depicted in Fig. 1(b) with all other parameters fixed at the following values: $\varepsilon_A = \varepsilon_{sub} = 12$, $\varepsilon_C = -40$, $w_B = 0.1\lambda_0$, $d_{AB} = d_C = 0.02\lambda_0$, where λ_0 is the wavelength of incident light in free space. In our calculations we fixed w_B and vary w_A to change P. According to the phase diagram depicted in Fig. 1(b), we find that the entire system becomes perfectly transparent when the geometrical and material parameters satisfy certain conditions. This is quite surprising at first glance, since the transmittance of a standing-alone C layer on the substrate is only $\sim 20\%$. However, with an additional AB layer put on its top, we can identify two main EM bands with transmittance values close to 100%.

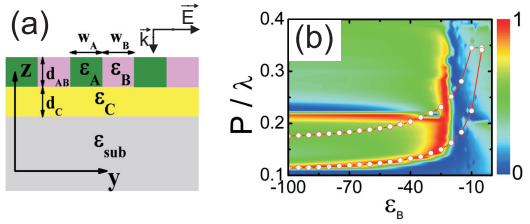

Fig. 1. (a) Schematic illustration of the proposed structure. (b) Transmittance (colorful scale) as the function of ε_B and P/λ. All other parameters are fixed, as described in the text.

We find that the discovered transparency phenomenon can be explained by the scattering cancellation mechanism in the same spirit as in [8]. Since the transparency region is where $P << \lambda_0$, we homogenize the composite AB layer based on the effective medium theory [10]. Such approximation greatly simplifies our considerations but helps capture the main physics. In the long wavelength limit, for the particular polarization $\mathbf{E}||y$, the effective permittivity of the AB layer can be obtained by:

#172483 - $15.00 USD Received 12 Jul 2012; revised 11 Sep 2012; accepted 12 Sep 2012; published 20 Sep 2012

$$\frac{1}{\varepsilon_{AB}} = \frac{1}{\varepsilon_A} \cdot \frac{w_A}{P} + \frac{1}{\varepsilon_B} \frac{w_B}{P}. \tag{1}$$

We can then employ the standard transfer-matrix-method (TMM) [11] to analytically calculate the transmittance/reflectance coefficients through the whole layered structure, e.g. air/AB/C/substrate.

$$\begin{pmatrix} t \\ 0 \end{pmatrix} = Q \cdot \begin{pmatrix} 1 \\ r \end{pmatrix}. \tag{2}$$

where $t = Q_{11} - Q_{12}Q_{21}/Q_{22}$ and $r = -Q_{21}/Q_{22}$ are respectively the transmittance and reflectance coefficients, and Q is the 2×2 scattering matrix of the system. In the ideal lossless case perfect transparency corresponds to zero reflectance, i.e., $Q_{21} = 0$. Therefore, analysis of function Q_{21} will give us some directions for achieving transparency. Through straightforward but tedious calculations, we found that:

$$\begin{aligned} Q_{21} \quad &= \left(1 - \tfrac{1}{\sqrt{\varepsilon_{sub}}}\right) + i \cdot \left[\left(\tfrac{1}{\sqrt{|\varepsilon_C|}} + \tfrac{\sqrt{|\varepsilon_C|}}{\sqrt{\varepsilon_{sub}}} \right) \tanh\left(\sqrt{|\varepsilon_C|} d_C/\lambda_0 \right) \right] + \\ &\quad + i \cdot \left[\left(\tfrac{1}{\sqrt{\varepsilon_{AB}}} - \tfrac{\sqrt{\varepsilon_{AB}}}{\sqrt{\varepsilon_{sub}}} \right) \tan\left(\sqrt{\varepsilon_{AB}} d_{AB}/\lambda_0 \right) \right] - \\ &\quad - \left(\tfrac{\sqrt{\varepsilon_{AB}}}{\sqrt{|\varepsilon_C|}} + \tfrac{\sqrt{|\varepsilon_C|}}{\sqrt{\varepsilon_{AB}}\sqrt{\varepsilon_{sub}}} \right) \tan\left(\sqrt{\varepsilon_{AB}} d_{AB}/\lambda_0 \right) \tanh\left(\sqrt{|\varepsilon_C|} d_C/\lambda_0 \right) \end{aligned} \tag{3}$$

We note that all terms in Eq. (3) have clear physical interpretations. The first two terms represent scattering from the semi-infinite substrate and the C layer, respectively. The third term is clearly contributed by the AB layer. Finally the forth term results from multiple scattering in all layers. It is obvious from Eq. (3) that the presence of the AB layer can generate additional scattering terms (the last two ones) to cancel those contributed by the C layer and the semi-infinite substrate. However, different from [8], we find that function Q_{21} is complex having both real and imaginary parts. Therefore, satisfying condition $Q_{21} = 0$ by tuning only one parameter ε_{AB} is not guaranteed. To understand the phase diagram presented in Fig. 1(b), we relax the perfect transparency condition. Instead of solving equation $Q_{21} = 0$ accurately, we vary parameter w_A, while keeping all other parameters fixed, to find the solutions that minimize quantity $|Q_{21}/Q_{22}|$. In this analysis we can omit Q_{22} since it is a smooth function of w_A with very large values, so the important parameter determining the reflectance is apparently Q_{21}. The solutions obtained by the minimization procedure are depicted in Fig. 1(b) with the open circles. We find the FEM simulated transparency bands match quite well with the minimization model results, indicating that the present discovered transparency is indeed governed by the scattering cancellation mechanism. Specifically, adjusting parameter w_A can efficiently modulate the scattering from the AB layer so that the reflectance from the system is minimized (see (Eq.) 3)), leading to the significantly enhanced EM wave transmittance.

The discrepancies between the full-wave simulations and model results are found mainly for the upper branch and in the right part of the graph. It is easily understandable since in these regions the structure cannot be considered deeply sub-wavelength, so that the effective medium description of the AB layer is not correct anymore. It is interesting to note that, while the effective medium model considerations do not guarantee the existence of perfect transparency, the full-wave simulations on realistic structures show that the maximized transmittance in each case can indeed be almost 100%.

#172483 - $15.00 USD Received 12 Jul 2012; revised 11 Sep 2012; accepted 12 Sep 2012; published 20 Sep 2012

3. Transparent THz electrode

Although the illustrative example presented above is very particular, our approach can be expanded to any parameter set due to the generality of the involved formulae. Once the C layer properties are known, the AB-layer parameters can be deduced. Also, the concept is applicable to any EM frequency domain as long as the required material parameters can be realized. The most natural applications of our design are in the visible domain, where the permittivities of plasmonic metals are in the desired region (see Fig. 1). Nevertheless, to verify the concept experimentally we decided to apply it in the THz domain to avoid notorious fabrication challenges of nanophotonics.

In the low-THz region metals can be considered as almost perfect electric conductors. Their negative permittivities are typically much bigger in the absolute values than requested in Fig. 1. Therefore, we exploited the approach from [12] and mimicked plasmonic metals by designed THz MTMs based on sub-wavelength metallic meshes (as diluted metals). The detailed configurations of the THz MTM samples mimicking plasmonic metals B and C are shown in Fig. 2(a). For the mesh C the unit cell is a $50\mu m \times 50\mu m$ square. For the mesh B the unit cell is a $100\mu m \times 30\mu m$ rectangle. Each metallic line has width $4\mu m$ and thickness $200nm$.

The vertical cross-section of the sample is shown in Fig. 2(b). The semi-infinite substrate is assumed as Si with $\varepsilon_{Si} = 11.7$, the $12\mu m$-thick SiO_2 layer (with $\varepsilon_{SiO_2} = 3.85$ [13]) is considered as a spacer between the two metallic meshes and a $200nm$-thick SiO_2 layer is placed on the very top for protection.

In accordance with the configuration from Fig. 1(a), we define the MTM B as the sandwich of mesh B between the SiO_2 cover layer and a half of the spacer layer. The MTM C is defined as the mesh C covered by a half of the spacer layer. The virtual interface between B and C MTMs is shown by the demarcation dashed line (see Fig. 2(b)). In the high frequency limit the MTMs should behave as a dielectric with the permittivity close to that of silica.

Due to the presence of a non-terminated metallic mesh, we assume that such MTMs can be assigned with a Drude-like behavior, similar to the diluted metal concept [12]. In order to retrieve their effective permittivities we first performed FDTD simulations to get the transmittance spectra. Then we fitted the simulation results with the Drude model. It resulted that the permittivities of the MTMs B and C can be respectively described by $\varepsilon_B = 3.85 - (3.06/f)^2, \varepsilon_C = 3.85 - (4.98/f)^2$, with f denoting the frequency in THz. For the $f = 0.6$THz these formulae give us $\varepsilon_C \sim -65$ and $\varepsilon_B \sim -22$, indicating that designed MTMs can indeed mimic plasmonic metals with the negative values of permittivity being in the desired range

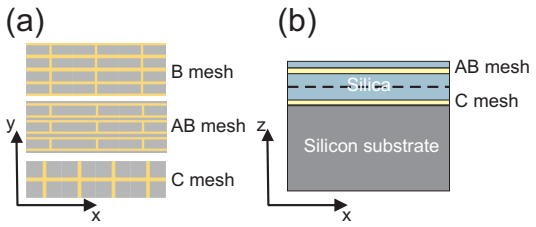

Fig. 2. The unit cells as seen from the xy plane (a) and the proposed structure in xz plane (b). The **E** field is parallel to the y-axis. The AB mesh is obtained by sectioning the B mesh and introducing a stripe of material, the A layer, in the cut. The width of the A stripe is calculated such that to reach the desired effective permittivity. The dotted line represents the demarcation between the C and the AB metamaterial. Not on scale.

The next step is to design the AB layer. Since the mesh B has the lattice constant of $30\mu m$

#172483 - $15.00 USD Received 12 Jul 2012; revised 11 Sep 2012; accepted 12 Sep 2012; published 20 Sep 2012

along the y-axis, we must take the width w_B of stripe B as $n \times 30\mu m$ with n and integer when designing the AB layer. Otherwise the stripes B may not have the same properties as the original B mesh. Taking material A as silica, we set the widths of stripes A and B as $w_A = 10\mu m$ and $w_B = 30\mu m$ (see Fig. 2(a)). The AB layer thus obtained is placed on top of the C layer and we obtain the final design shown in Fig. 2(b). Through comparing the transmission spectra calculated with a homogenous effective-medium slab and full-wave simulations on the realistic AB structure, we found that the effective permittivity of the AB layer can be given by $\varepsilon_{AB} = 3.85 + 4.19/(0.74^2 - f^2)$. The resonance behavior of ε_{AB} ensures that there must be a frequency where it exhibits the desired value to make the whole structure transparent.

We performed FDTD simulations [14] based on realistic material parameters to study the transmittance spectrum $T = |S_{21}|^2$ through the designed structure. In our calculations all materials are assumed to be non-magnetic $(\mu = \mu_0)$, and the dielectric function of aluminum is described using the Drude model with parameters from [15]. In the case of a bare Si substrate of $530\mu m$ thickness the calculated transmittance is $\sim 70\%$. As expected, the C layer greatly diminishes the transmittance down to $\sim 30\%$. However, by putting the AB layer on top of the C layer we can reach almost 100% transmittance at $0.57THz$ (see Fig. 3(a)). It is worth noting that the incident wavelength is roughly 40 times larger than the thickness $(\sim 12.7\mu m)$ of the AB layer. Yet, by appropriately adjusting the material and geometric parameters of such thin AB layer, we can make its scattering strong enough to completely compensate the scattering from the C layer, leading to nearly perfect transparency. The entire device thus combines high optical transmittance with good in-plane electric conductivity, which is highly desired in many optoelectronic applications.

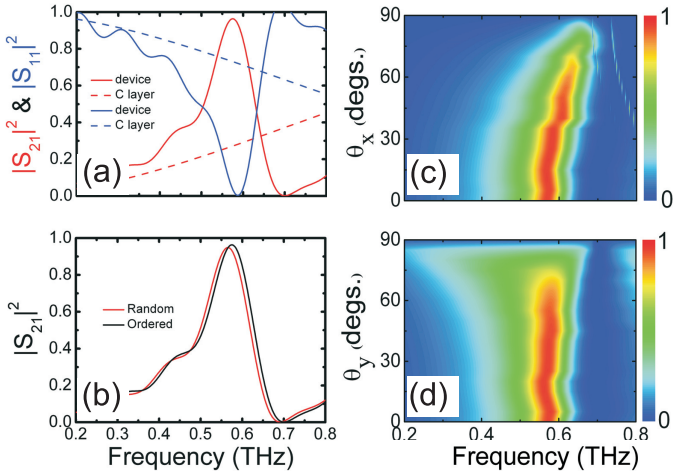

Fig. 3. (a) simulated transmittance (red) and reflectance (blue) spectra of the proposed configuration in Fig. 2 (solid line) as well as of the simple C-layer mesh (dash line). (b) the compared transmittance of ideal and randomized structure. (c) and (d) respectively represent the behavior of the structure when varying the incidence angle in the (x,z) plane and (y,z) plane. The incident field is polarized along the Y axis

We also simulated the imperfection tolerance of the design by introducing deviations from the ideal structure parameters. In Fig. 3(b) the transmittance results are shown for ordered and randomized structures. The randomness was introduced by varying the w_A within $10 \times (1 \pm 40\%)\mu m$ while keeping the other parameters constant. Although there is a slight shift of about 10GHz in the spectra, it is basically negligible from the practical point of view. Such

#172483 - $15.00 USD Received 12 Jul 2012; revised 11 Sep 2012; accepted 12 Sep 2012; published 20 Sep 2012

pronounced tolerance for parameters changes is extremely important for implementing the device in real-life applications, where the fabrication imperfections and the in-situ variations can otherwise hinder its functionality.

The proposed transparency is rather insensitive to the incidence angle. The simulated transmittance as function of incidence angle and frequency f are shown in Figs. 3(c) and 3(d) for θ_x and θ_y respectively. The transparency is stable within the extended range of incidence angles $\theta_y \sim 60^\circ$ and $\theta_x \sim 35^\circ$.

4. Transmission line model

Another view on the the transparent electrodes performance can be given using the transmission line analogy that is applicable in the long-wavelength regime. The transmission line (TL) approach is a common language in the microwave engineering. It provides important insight to how the metamaterial surface should be modified in order to reach the desired functionality, for example, to modify the resonant frequency, bandwidth or transmittance amplitude.

Propagation of a plane wave in a homogeneous dielectric may be considered as propagation (for example, along z-axis) of the fundamental mode in a dielectric filled rectangular waveguide $(a \times b)$ with the perfect electric (x-) and perfect magnetic (y-) boundaries [16, 17]. In such homogeneous transmission line the x-polarized electric field E is connected with the voltage through $V = aE$ and y-polarized magnetic field H is linked with the current through $I = bH$. The relation between the electric and magnetic fields is described by the wave impedance $\eta = E/H = \sqrt{\frac{\mu\mu_0}{\varepsilon\varepsilon_0}}$, while the relation between the voltage and current is described through the characteristic impedance $Z_C = \frac{V}{I} = \frac{aE}{bH} = a\eta/b$. The transmittance through a single interface (see Fig. 4(a)) between two dielectrics (η_1 and η_2) is equal to

$$T = \frac{4\eta_1\eta_2}{(\eta_1+\eta_2)^2} \tag{4}$$

For a bare silicon substrate $(\eta_2 = 0.29Z_0)$ in air $(\eta_1 = Z_0 = 120\pi\Omega)$ the transmittance is $T = 0.7$.

A dielectric layer (with impedance η) of thickness d between two other semiinfinite dielectrics (η_1 and η_2) is analogous to a short transmission line section inserted between two other transmission lines (see Fig. 4(b)). The transmittance through it can be calculated with the Airy formulas [18]

$$T = \frac{\eta_1}{\eta_2}\left|\frac{t_{1\eta}t_{\eta 2}}{1-r_{\eta 1}r_{\eta 2}\exp(ikd)}\right|^2 \tag{5}$$

The meaning of the amplitude transmittance and reflectance coefficients $t_{1\eta}, t_{\eta 2}, r_{\eta 1}, r_{\eta 2}$ is clear from the central panel of Fig. 4(b). The exponential term accounts for the phase advance upon propagation through the layer.

For our structure we used a very thin dielectric layer $d = 12\mu m$ comparing to the wavelength of electromagnetic radiation $(\lambda \sim 600\mu m)$, so the working frequency is far lower than the first Fabry-Perot resonance and the transmittance is almost the same as the one through the silicon-air interface.

Adding an electrically thin (thickness is much smaller than the wavelength) structured metallic layer (or metamaterial surface) to the interface between two dielectrics (see Fig. 4(c)) is equivalent to adding shunt impedance $Z = a\eta_{eq}/b$, which is an impedance of the unit cell, at the point where the transmission lines are connected. The amplitude transmittance t and reflectance r coefficients are then:

#172483 - $15.00 USD Received 12 Jul 2012; revised 11 Sep 2012; accepted 12 Sep 2012; published 20 Sep 2012

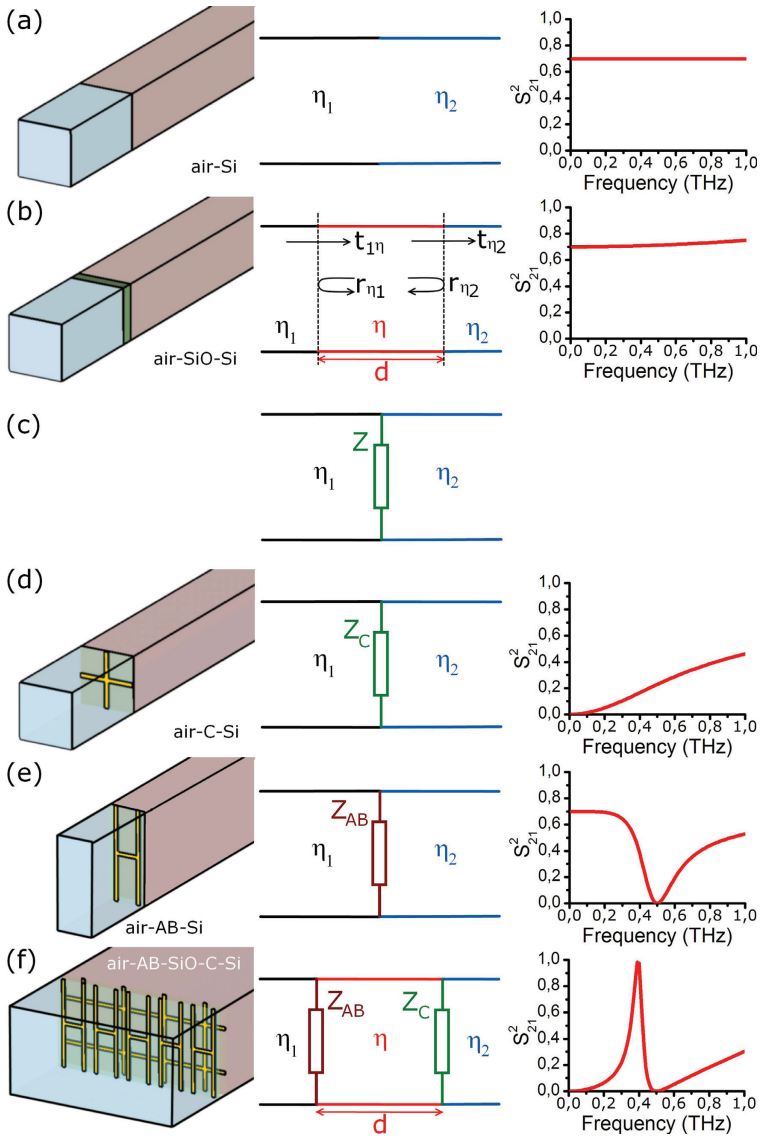

Fig. 4. Structures, their circuit models and transmittance spectra. (a) Single interface between two dielectrics; (b) thin dielectric layer between two homogeneous dielectrics; (c) equivalent transmission line model for the thin layer; (d) layer C and the TL model; (e) layer AB and the TL model; (f) complete system and the TL model. The incident radiation is normal to the structures with the **E** field parallel to the middle line of the ”H”-like structure.

#172483 - $15.00 USD Received 12 Jul 2012; revised 11 Sep 2012; accepted 12 Sep 2012; published 20 Sep 2012

$$t = \frac{\frac{2}{\eta_1}}{\frac{1}{\eta_1}+\frac{1}{\eta_2}+\frac{1}{\eta_{eq}}} \quad (6)$$

$$r = \frac{\frac{1}{\eta_1}-\frac{1}{\eta_2}-\frac{1}{\eta_{eq}}}{\frac{1}{\eta_1}+\frac{1}{\eta_2}+\frac{1}{\eta_{eq}}}, \quad (7)$$

where the equivalent wave impedance $\eta_{eq} = bZ/a$. A highly conductive layer $(Z = 0)$ makes a short circuit, so the incoming wave is fully reflected back. A very high impedance $(Z >> \eta)$ is equivalent to an open circuit and the wave is transmitted through the interface as there is no impedance (no any thin layer) at all. In the case of a metamaterial surface its impedance can be qualitatively estimated by constructing an equivalent LRC-circuit. The simple modeling is that a wire along the electric field corresponds to an inductance and a resistance, and a dielectric gap gives a capacitance.

Let's now consider our design parts C, AB and the whole structure ABC - by the TL approach. To calculate the transmittance through two thin metamaterial layers separated with a dielectric one, we should use Eq. (5) with the reflectance and transmittance coefficients modified according to Eqs. (6) and (7). For the qualitative explanation we neglect the Ohmic losses.

The mesh C in our design consists of crossing wires (Fig. 4(d)). Assuming that we can neglect the capacity between the wires it's impedance $Z_C = -i\omega L_C$ is purely determined by inductance L_C (we use the optical convention for the phase factor $\exp(-i\omega t)$). Consequently, at low frequencies impedance Z_C is low comparing to $\eta_{1,2}$, and the layer C acts as a high-frequency filter (see the right panel of Fig.4(d).

The layer AB (Fig. 4(e)) consists of short vertical metal wires (inductance L_{AB}) with a gap between horizontal wires (capacitance C_{AB}). Its impedance $Z_{AB} = -i(\omega L_{AB} - \frac{1}{\omega C_{AB}})$ is high at low frequencies $(\omega << \frac{1}{\sqrt{L_{AB}C_{AB}}})$ and at high frequencies $(\omega >> \frac{1}{\sqrt{L_{AB}C_{AB}}})$, but close to zero near the resonance $(\omega_{AB} = \frac{1}{\sqrt{L_{AB}C_{AB}}})$. Thus the layer AB itself acts as a rejection filter prohibiting transmission in a narrow band near the resonance - the right panel of Fig. 4(e).

Together the ABC system corresponds to an equivalent transmission line shown in Fig. 4(f) if we assume, for simplicity, that the mutual inductance between the two layers can be neglected. We regard the AB and C layers as two impedances (see Fig. 1) connected in parallel and thus having the total impedance:

$$Z_{total} = \frac{Z_1 Z_2}{Z_1 + Z_2} = -i\frac{\omega L_C(\omega L_{AB} - \frac{1}{\omega C_{AB}})}{\omega(L_C + L_{AB}) - \frac{1}{\omega C_{AB}}} \quad (8)$$

Impedance Z_{total} is zero (so no transmission) at the AB resonance frequency $\omega_{AB} = \frac{1}{\sqrt{L_{AB}C_{AB}}}$. In contrary it is very large at frequency $\omega_{ABC} = \frac{1}{\sqrt{(L_{AB}+L_C)C_{AB}}} < \omega_{AB}$ that leads to a very high transmission close to 100%. We should emphasize that the ABC structure is not only able to recover the transmission from very low to the order of that at the silicon-air interface, but also to overcome this level and provide theoretically full transparency.

Another explanation of this peak (the Fabry-Perot picture) can be given if we account for a thin dielectric layer between the metallic AB and C meshes. As we mentioned before, the thickness of the dielectric (silica) between AB and C layers $d = 12\mu m$ is much smaller than the wavelength of the used THz radiation $(600\mu m)$, so the silica layer itself cannot give a high transmission satisfying the first Fabry-Perot resonance condition: the total phase advance during the back and forth propagation in the resonator should be equal to 2π. However, the phase of the electromagnetic wave experiences large changes upon the reflection from the AB and C

#172483 - $15.00 USD Received 12 Jul 2012; revised 11 Sep 2012; accepted 12 Sep 2012; published 20 Sep 2012

meshes near frequency ω_{ABC}, so it becomes possible to satisfy the Fabry-Perot phase condition even with a very small dielectric layer. Consequently, we observe a high transmission peak [7].

The TL approach gives not only a simple explanation of the observed effects, but also a good advice on the structure modification in order to reach the desired functionality. For example, if one wishes to decrease the frequency of the high transmission peak, one has to increase capacitance C_{AB} by making, for example, the gap between the horizontal wires smaller.

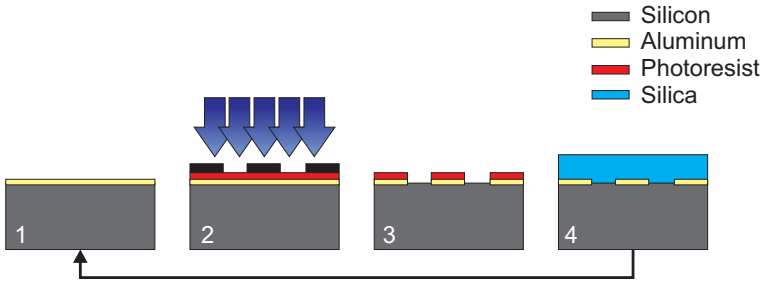

Fig. 5. Schematic of the fabrication procedure, not on scale. (1) Initial wafer with deposited Al; (2) photoresist deposition and masked optical exposure for defining the structures; (3) develop of photoresist and Al etch; (4)removal of the photoresist and deposit silica layer. After this step, the process is repeated for the next layer.

5. Fabrication

Having got the optimized design we fabricated the THz samples. The structure was erected on a high-resistivity silicon (Si) wafer. The choice for the substrate was due to its high transmission at the low THz frequencies, thus allowing a good signal-to-noise ratio.

The fabrication procedure is presented schematically in Fig. 5. The first step consists in depositing 200nm of aluminum (Al) on top of the Si substrate. This layer is the one where the metallic mesh will be etched in.

Next, the deposition, exposure and development of the photosensitive polymer that acts as an etching mask is performed. Since the resolution of the structure is in the order of microns, the optical lithography was the choice for exposing the structure. At this point, the mesh is defined in polymer and, using dry metal etching in plasma of HBr and Cl_2 we transferred the pattern to the metal beneath. We decided to use the etching technique instead of the more widely spread lift-off one in order to have better control over the structures geometrical dimension.

The dry etching was performed with an inductive coupled plasma reactive ion etching (ICP-RIE) machine. The etching starts with a 20s breakthrough step for removing native Al_2O_3 made at a Cl_2 flow of 20sccm with a platen power of 120W and a coil power of 600W. The next step, the etching of the Al layer, is made in a mixture of Cl_2/HBr 25/15sccm with platen and coil powers of 100W and 500W respectively. The etching time is 1 minute. After the etching of the Al layer, a 5 minutes O_2 plasma etching is performed in order to remove the polymer mask. At this point, the first layer is fabricated, Fig. 6(a).

The next step is the deposition of silica using a plasma enhanced chemical vapor deposition (PECVD) machine. Using an atmosphere of $SiH_4/N_2O/N_2$ maintained by a constant flow of $12/1420/392sccm$ respectively at 550mtorr pressure and power of 60W, we deposited $12.5\mu m$ of silica on top of the mesh layer. In order to obtain as high transmission as possible, the thickness of silica needs to be very well controlled thus, before the deposition, several tests were made to ensure the correct reading of the deposition rate, uniformity and stability. The deposition rate was of 81nm/min with less than 1% uniformity thus making a deposition time

#172483 - $15.00 USD Received 12 Jul 2012; revised 11 Sep 2012; accepted 12 Sep 2012; published 20 Sep 2012

of ca. 2h30min for the 12.5μm thick silica layer.

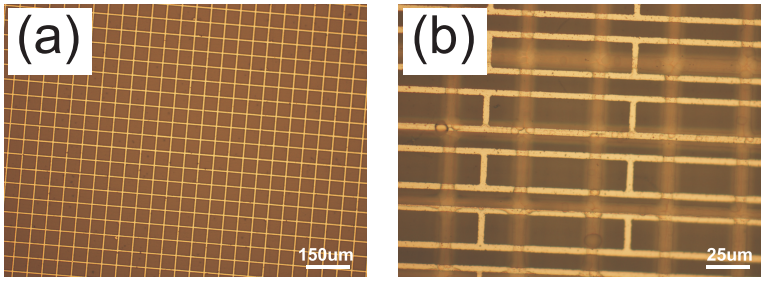

Fig. 6. Fabrication results. (a) Bottom layer; (b) top layer. The shadow of the bottom layer can be distinguished in the background.

Once the silica layer is deposited, the first steps are repeated with the only difference of having to align the second exposure to the first one (see Fig. 6(b)). The last fabrication step consists in depositing a thin 200nm silica layer on top of the structure using the same recipe as for the initial 12.5μm spacer.

6. Characterization

We characterized the fabricated samples using a T-Ray 4000 THz time-domain spectroscopy system. For every sample 10.000 waveforms were recorded with the scan rate of 100 Hz and the average of all the waveforms was then used for further investigation.

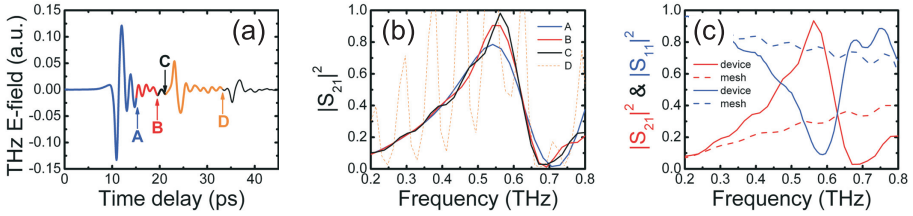

Fig. 7. Measured transmittance and reflectance intensity data. (a) Various pulse lengths and (b) their respective transmittance spectra showing the importance of correctly defining the cutting time-point; (c) transmittance (red) and reflectance (blue) for both the whole ABC device (solid lines) and C MTM layer (dashed). The averaged data for four devices and two mesh samples are presented.

Due to multiple reflections in the Si substrate the main pulse is closely followed by ripples from multiple reflections in the thin silica layer, Fig. 7(a). The THz transient signals were cut after careful analysis of the fourier transformed spectra. A too short pulse cut leads to significant loss of transmitted intensity, see points A, B, C in Fig. 7(a) and corresponding transmittance spectra in Fig. 7(b). On the other hand, in case of a too long pulse length (point D), the reflected signal from the back of the substrate causes huge Fabry-Perot oscillations that make the interpretation of the results difficult (see D line in Fig. 7(b)). Once the optimum cutting length was obtained, the reference signal is cut accordingly. The transmittance measurements were normalized to transmittance through the Si substrate with 12.5μm of silica characterized for referencing. The reflected signal was normalized to the one of an Al mirror, considered to be a perfect reflector ($|S_{11}|^2 \simeq 100\%$) at THz wavelengths.

Figure 7(c) shows both normalized transmittance and reflectance spectra for the complete

#172483 - $15.00 USD Received 12 Jul 2012; revised 11 Sep 2012; accepted 12 Sep 2012; published 20 Sep 2012

ABC device and C mesh samples. As expected quite low C mesh transmittance is greatly improved by cancelation of scattering with the help of the AB layer.

The direct comparison of modelling and characterization results (Fig. 8) exhibits their excellent agreement. The insignificant quantitative deviations of results are mainly due to the difficulty of perfectly finding the optimum pulse cutting length in measurements. Because of the inherent noise in the spectra and slight variations in the Si substrate thickness we cut the time domain signal at a different time-point than in simulation. In the same time, the level of the transmittance peak is greatly influenced by the pulse length due to the cavity effect that takes place in the silica layer (see Fig. 7(b)). Another factor that affects the transmission is the possible losses in the silica layer. The slight frequency shifts of $\sim 10GHz$ in the transmission peak position can be attributed to fabrication imperfections (see Fig. 3(b)).

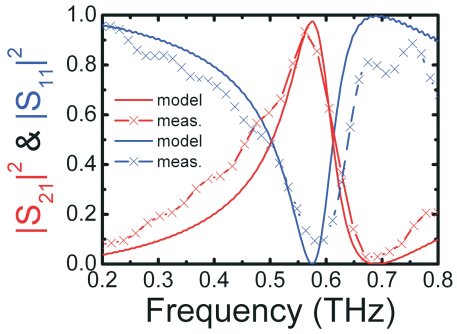

Fig. 8. Transmittance and reflectance data comparison. Full lines are the simulated results. The difference between the transmittance max amplitude is mainly due to the difficulty in finding the optimum cutting point as well as neglecting the losses in the silica layer in simulations.

7. Conclusion

In conclusion, we presented a simple mechanism to obtain transparent electrodes on a substrate. The metal electrode transmittance can be improved by canceling the scattering from a metallic film with the help of a metamaterial-inspired composite layer on top of the structure. The present mechanism is insensitive to structural disorders and broad variation of incidence angles. We also provide a transmission line model clearly explaining the effect of improved transparency in terms of combination of impedances from each structural part. The concept was successfully verified in THz regime, with optical plasmonic metals mimicked by carefully designed mesh-like MTMs. Results have been verified experimentally with good quantitative correspondence with the simulated ones.

This approach, although demonstrated here for the THz regime, can be extended to other important frequency domains, e.g. the visible range, where demanding applications of transparent electrodes in photovoltaic cells, touch screens and other display devices exist. The design proposed here is only applicable to one particular in-plane E field polarization, however it can be easily generalize to exhibit in-plane isotropic properties.

Acknowledgments

R.M., M.Z., A.L. acknowledge the FTP THzCOW project for partial financial support. Z.Y.S, Q. H. and L. Z. thank the financial supports from NSFC (60990321, 11174055), Program of

#172483 - $15.00 USD Received 12 Jul 2012; revised 11 Sep 2012; accepted 12 Sep 2012; published 20 Sep 2012

Shanghai Subject Chief Scientist (12XD1400700) and MOE of China (B06011). A.A. acknowledges the FTP GraTer project for partial financial support.

#172483 - $15.00 USD Received 12 Jul 2012; revised 11 Sep 2012; accepted 12 Sep 2012; published 20 Sep 2012